Journal of Civil Structural Health Monitoring (2024) 14:1017–1033
https://doi.org/10.1007/s13349-024-00769-x

ORIGINAL PAPER

Time-lag effect of thermal displacement and its compensation method for long-span bridges

Hong-Li Zhou[1] · Guang-Dong Zhou[1] · Zheng-Qi Qiao[1] · Bin Chen[2] · Jin-Lin Hu[1]

Received: 18 May 2023 / Accepted: 10 January 2024 / Published online: 22 February 2024

Abstract
The time-lag effect between temperature and thermal displacement may induce the displacement-based safety assessment results of long-span bridges to derivate from the truth. In this paper, the typical characteristics of the time-lag effect between temperature and thermal displacement are firstly investigated by using the synchronously monitored temperature and displacement data from a long-span steel box-girder arch bridge. And then, the inherent reasons of the time-lag effect are found out by employing the Kendall correlation coefficient. Following that, a general method derived from the Bayesian function registration model and the Z-mixture preconditioned Crank-Nicolson algorithm is proposed to compensate the time-lag effect. Finally, the proposed compensation method is verified by data from three bridges and compared with the traditional method achieved through shifting a fixed time interval. The results show that thermal displacement may be ahead of or lag behind temperature, depending on the temperature and thermal displacement of concern. The lag time varies from a few minutes to several hours with temperature and displacement variables, as well as time instants. The time-lag effect between temperature and thermal displacement is caused by the asynchronous change of the dominant temperature for the specific thermal displacement and other temperatures because of different material thermodynamic parameters and geometric characteristics of different bridge components. The developed compensation method can completely eliminate the time-lag effect between temperature and thermal displacement of various long-span bridges without any pre-correlation analysis and prior knowledge. The correlation between temperature and thermal displacement compensated by the method proposed in this paper is much stronger than that compensated by the traditional method.

Keywords Structural health monitoring · Long-span bridge · Temperature effect · Thermal displacement · Time-lag effect

1 Introduction

Structural health monitoring (SHM) has been widely accepted as an effectively approach to ensure the structural safety, serviceability and reliability of long-span bridges. Various parameters monitored by SHM systems are adopted for structural damage detection and performance evaluation [1–4]. Among them, displacement is a typical one and has been flexibly used by many researchers [5–7]. However, in addition to structural damages and operational loads such as wind load and vehicle load, temperature can also induce remarkable displacement in long-span bridges. Sometimes, the displacement caused by temperature may exceed the displacement caused by structural damages or operational loads [8, 9]. Therefore, in order to use displacement to reliably indicate damages in long-span bridges, it is significant to thoroughly understand the correlation between temperature and displacement. As a result, the displacement caused by temperature could be reasonably separated from the monitored displacement results and the displacement caused by damages is discernible.

In recent decades, intensive research activities regarding the correlation between temperature and thermal displacement of long-span bridges have been carried out. Li et al. provided an excellent review on the temperature distribution and the temperature actions of various types of bridges, including beam bridges, arch bridges, cable-stayed bridges, and suspension bridges [10]. Specifically, as early as 1989, Potgieter and Gamble investigated the effects of nonlinear

✉ Guang-Dong Zhou
zhougd@hhu.edu.cn

[1] College of Civil and Transportation Engineering, Hohai University, Nanjing, People's Republic of China

[2] Zhejiang University City College, Hangzhou, People's Republic of China

temperature distributions in bridge structures resulting from solar radiation and other related weather parameters [11]. With the development of SHM technology, the temperature distribution and its impact on long-span bridges have been widely studied based on long-term monitored data. Ni et al. discussed the influence of temperature on modal frequencies and longitudinal displacement earlier and developed influential methods to establish correlation models between temperature and temperature-induced responses [12, 13]. Subsequently, Catbas et al. found that temperature has a significant effect on the overall system reliability of long-span bridges [14]. Xu et al. studied the statistical relationship between effective temperature and displacement of the Tsing Ma Bridge using data recorded in the equipped SHM system [8]. Kromanis and Kripakaran proposed a data-driven strategy for predicting thermal response of structures from distributed temperature measurements [15]. Yang et al. carried out a monitoring-based analysis of temperature-induced girder deflection for a combined highway and railway cable-stayed bridge and formulated the correlation between the structural temperature and the girder deflections [16]. Zhou et al. proposed a closed-form thermal correlation model based on monitoring data and applied it to a bridge to verify the model universality [17]. Zhou et al. deduced the analytical formulas to describe the thermal deformation of suspension bridges and used eight real long-span suspension bridges as examples to verify the results [9]. Those research works provide valuable information for establishing the relationship between temperature and thermal displacement.

Because of the complication of material thermodynamic properties and structural geometric configurations of long-span bridges, the change of structural temperature and the variation of structural displacement may be asynchronous, which is term as the time-lag effect. The time-lag effect has been found in many monitored temperature and displacement data from different bridge health monitoring systems [7, 18, 19]. Westgate et al. discussed the phenomenon of the time-lag effect in long-span bridges and attributed it to the difference of thermodynamic features between concrete and steel [20]. Wang et al. observed the time-lag effect between the surface solar radiation intensity and structural effective temperature [21]. The time-lag effect will cause notable hysteresis loops between temperature and thermal deformation. As a result, there is no obvious linear temperature–displacement correlation any more, which in turn reduce the reliability of displacement-based damage identification and safety assessment results [22]. Thus, in order to establish more accurate temperature–displacement correlation models for long-span bridges and obtain more reliable displacement-based damage detection results, the time-lag effect should be carefully compensated.

At present, the time-lag effect is arbitrarily compensated by shifting a fixed time interval in most researches. For examples, Guo et al. put the temperature data 45 min behind the displacement data to enhance the linearity [23]; Yang et al. shifted the deflection of the main girder of a combined highway and railway cable-stayed bridge for 2.2 h to mitigate the time-lag effect [24]; Wang et al. used the historical average lag time to remove the time-lag effect [21]; Ju et al. adopted 2.8 h and 2.9 h to eliminate the temperature time-lag effect in bridge tower data, respectively [22]. However, due to the lag time may change with time and be variable between different temperature and displacement variables, these compensation methods of shifting a fixed time interval cannot completely eliminate it. At the same time, the intrinsic reason inducing the time-lag effect has not yet been captured. Therefore, it becomes necessary to fully study the mechanism of the time-lag effect and develop a more accurate and flexible compensation method to address it. In this paper, the characteristics of the time-lag effect between temperature and thermal displacement are carefully investigated based on long-term monitored temperature and displacement data recorded by a SHM system equipped on a long-span steel box-girder arch bridge. The inherent reason leading to the time-lag effect is extracted. Following that, a general method is proposed to compensate the time-lag effect, and data obtained from three bridges are adopted to verify its effectiveness. The research results can provide reference value for modeling temperature–displacement correlation and conducting displacement-based structural safety assessment of long-span bridges.

2 Characteristics of the time-lag effect

2.1 Temperature and response data

The synchronously temperature and response data (i.e. displacements) used for analysis obtained from a SHM system installed on a three-span continuous steel box-girder arch bridge, as shown in Fig. 1. Each of the three spans is 210 m. The arch system, which is supported by the V-shaped thin-wall pier, is composed of the external-inclined main arch rib, the internal-inclined auxiliary arch rib, the transversal brace between the main and auxiliary rib, and the transversal vault connector between the two auxiliary arch ribs. Thirty-eight suspenders are adopted to transfer the load from the main girder to the arch system. The main girder is a steel-box girder with a uniform cross-section. The precast concrete slab with a thickness of 260 mm is used as the bridge deck system. The main rib, auxiliary rib, transversal brace, transversal vault connector, suspenders and main girder make the load transfer extremely complex. In order to ensure the safety of the bridge, a versatile SHM system was installed to monitor the external environment, operation load and structural responses in real time [25].

Fig. 1 Overview of the steel box-girder arch bridge

Digital temperature sensors are adopted to monitor structural temperatures in the main arch rib, suspenders and main girder, as shown in Figs. 2 and 3. The subscript in Fig. 2 represents the number of the monitored section and the number in the bracket denotes the sensor number; while the first subscript in Fig. 3 indicates the monitored section number and the second subscript is the sensor number. The resolution of the digital temperature sensor is 0.0625 °C, and the measurement range is − 55 to 125 °C. The sampling period is set as 1 min.

The vertical displacement of the main girder is monitored by connecting pipes combined with pressure sensors. Twenty pressure sensors are installed in each quarter span and mid-span, as shown in Fig. 4. These sensors are divided into two groups. In each group, the pressure sensor located on the top of the pier, where the vertical displacement is almost equal to zero, is selected as the reference sensor. The real vertical displacement is equal to the measured result of the pressure sensor minus the measured result of the reference sensor. The measuring range of the pressure sensor is 1000 mm, and the measuring accuracy is ± 0.065%. The

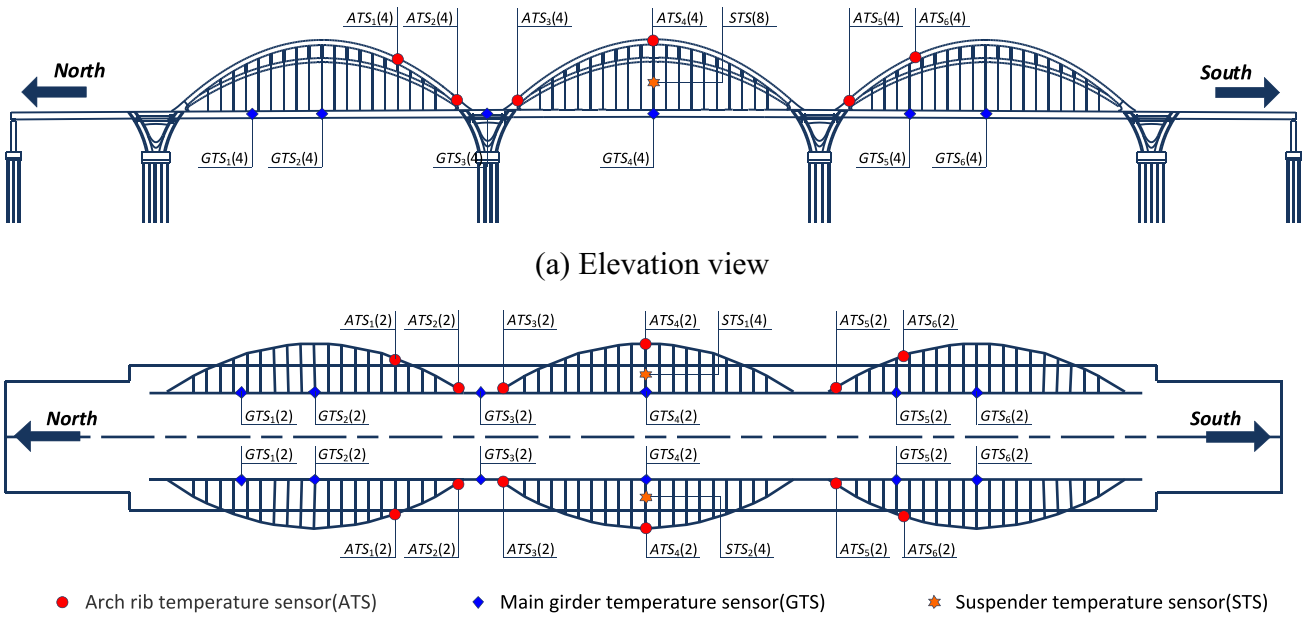

Fig. 2 Layout of temperature sensors

sampling period of pressure sensors is 10 s. The longitudinal displacement of the main girder is measured by two magnetostrictive displacement transducers, which are located at both ends of the main girder, as displayed in Fig. 4. The measuring range of the magnetostrictive displacement transducer is 7600 mm, and its resolution is 0.1 mm. The sampling period of the longitudinal displacement is also 10 s.

2.2 Data preprocessing

The sampling frequencies of monitored temperature and displacement data may be different, which brings difficulties to the discussion and compensation of the time-lag effect. Not only that, the monitored displacement, especially the vertical displacement, includes not only the part induced by temperature, but also the part caused by other factors, such as wind and vehicle load. In this paper, the following procedures are employed to extract the vertical and longitudinal displacement induced by temperature. The flowchart is shown in Fig. 5.

Step (1). The measured temperature and displacement are simultaneously averaged in a fixed time interval. Here, the 10 min is used. As a result, the sampling frequency of temperature and displacement is kept the same and the computational efficiency is improved. Furthermore, these dynamic parts induced by vehicle load and environmental vibrations and the measurement noises are deleted from the monitored displacement.

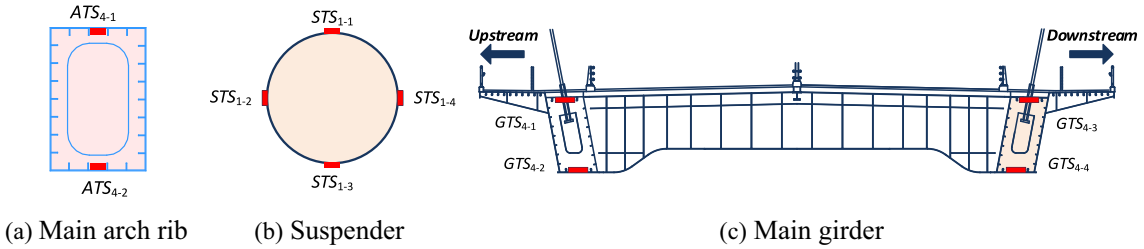

(a) Main arch rib (b) Suspender (c) Main girder

Fig. 3 Locations of temperature sensors on bridge components

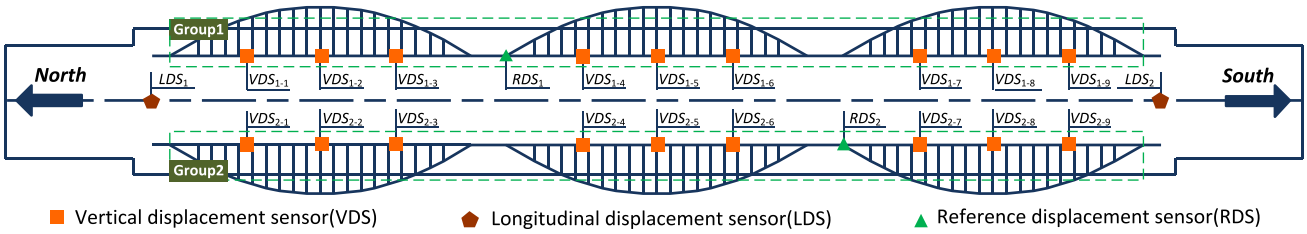

Fig. 4 Layout of displacement sensors

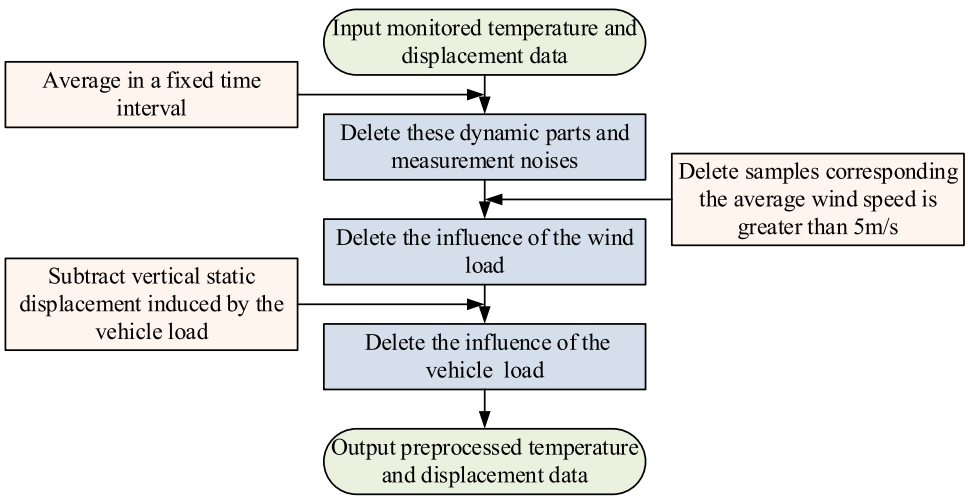

Fig. 5 Flowchart of data preprocessing

Step (2). These temperature and displacement samples are deleted when the average wind speed in 10 min is greater than 5 m/s, supposing that the wind-induced displacement can be ignored. As a consequence, the influence of the wind load is eliminated.

Step (3). The updated finite element model of the bridge is employed to calculate the vertical static displacement by using the vehicle load obtained from the weight in motion system as input [17]. Then, the vertical static displacement induced by the vehicle load can be eliminated.

2.3 Phenomenon of the time-lag effect

In general, the mean temperature or the effective temperature of a bridge is chosen as the representative temperature variables to perform temperature-based structural evaluation [26, 27]. For the employed long-span bridge, the mean temperature and thermal displacement in the middle cross-section of the middle span is calculated by Eqs. (1) ~ (7).

$$T_{mean} = \frac{1}{4}\left(AT_{mean} + ST_{mean} + GT_{u-mean} + GT_{l-mean}\right) \quad (1)$$

$$AT_{mean} = \frac{1}{4}\sum_{i=1}^{4} ATS_{4-i} \quad (2)$$

$$ST_{mean} = \frac{1}{4}\sum_{i=1}^{4} STS_{1-i} + \frac{1}{4}\sum_{i=1}^{4} STS_{2-i} \quad (3)$$

$$GT_{u-mean} = \frac{1}{2}\left(GTS_{4-1} + GTS_{4-3}\right) \quad (4)$$

$$GT_{l-mean} = \frac{1}{2}\left(GTS_{4-2} + GTS_{4-4}\right) \quad (5)$$

$$VD_{mean} = \frac{1}{2}\left(VDS_{1-5} - RDS_1 + VDS_{2-5} - RDS_2\right) \quad (6)$$

$$LD_{mean} = \frac{1}{2}\left(LDS_1 + LDS_2\right), \quad (7)$$

where T_{mean}, AT_{mean}, ST_{mean}, GT_{u-mean} and GT_{l-mean} represent mean temperatures in the whole cross-section, arch rib, suspender, upper surface of the main girder and lower surface of the main girder, respectively; ATS_{4-i}, ATS_{1-i}, ATS_{2-i} and GTS_{4-i} denote temperatures monitored by sensors ATS_{4-i}, STS_{1-i}, STS_{2-i} and GTS_{4-i} shown in Figs. 2 and 3, respectively; VD_{mean} and LD_{mean} are vertical mean displacement and longitudinal mean displacement, respectively; VDS_{1-5}, RDS_1, VDS_{2-5}, RDS_2, LDS_1 and LDS_2 denotes displacement measured by sensors VDS_{1-5}, RDS_1, VDS_{2-5}, RDS_2, LDS_1 and LDS_2 shown in Fig. 4, respectively.

The mean temperature in the whole cross-section and thermal displacement data of five continuous days in summer and winter are randomly selected to analyze. The time histories of displacement and temperature are plotted and compared in Fig. 6. And the corresponding lag times are listed in Table 1. In the figure, the subscripts *w* and *s* represent summer and winter, respectively. In the table, negative numbers indicate that the mean temperature lags behind the displacement, and vice versa. It can be seen from the two figures and the table that the time-lag effect is remarkable and similar in winter and summer. Specifically, vertical displacement is ahead of mean temperature in the whole cross-section; while longitudinal displacement lags behind

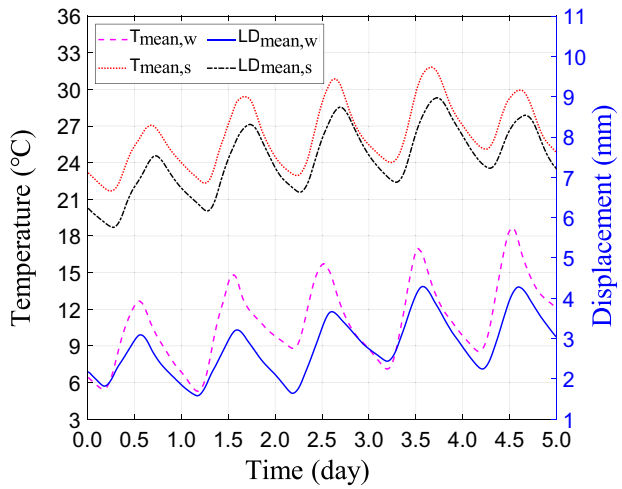

(a) Longitudinal displacement

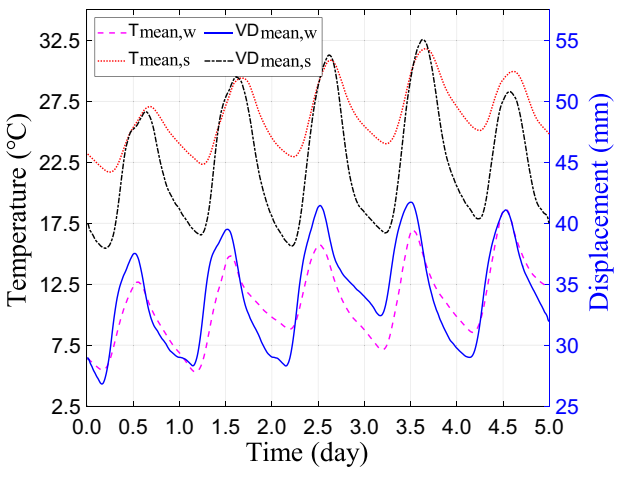

(b) Vertical displacement

Fig. 6 Time histories of mean temperature in the whole cross section and displacement

Table 1 Lag times between mean temperature and displacement (Unit: min)

Variables	Mean temperature vs. vertical displacement				Mean temperature vs. longitudinal displacement			
	Winter		Summer		Winter		Summer	
	Peak	Valley	Peak	Valley	Peak	Valley	Peak	Valley
Day 1	− 50	− 50	− 60	− 60	10	10	70	50
Day 2	− 50	− 40	− 80	− 20	60	0	90	50
Day 3	0	− 50	− 30	− 30	100	0	100	60
Day 4	− 30	− 30	− 50	− 20	80	0	90	80
Day 5	0	− 50	− 40	− 30	80	50	90	60
Average values	− 26	− 44	− 52	− 32	66	12	88	60

mean temperature in the whole cross-section. The time-lag effect is time-dependent. Furthermore, the lag times between vertical displacement and mean temperature in the whole cross-section and that between longitudinal displacement and mean temperature in the whole cross-section are different. The time-lag effect changes with thermal displacement variables. It can be concluded that the method of using a fixed time interval to arbitrarily compensate the time-lag effect is inadvisable.

2.4 Inherent reason of the time-lag effect

According to the thermodynamic theory, the thermal deformation of the material is completely synchronous with the temperature change, and there is no time-lag effect. However, noticeable time-lag effects between thermal displacement and temperature are found in monitored data. Therefore, careful investigation is required to capture the reason.

The time histories of mean temperatures in bridge components and thermal displacements are plotted in Figs. 7 and 8. It can be seen from these figures that, for the same mean temperature and thermal displacement, the characteristics of the time-lag effect are almost the same in summer and winter; but for different mean temperatures and thermal displacements, the properties of the time-lag effect are different from each other even in the same season. When taking a closer look, there is no obvious time-lag effect between the mean temperatures in the main arch rib and the suspender and vertical displacement, as shown in Fig. 7. But vertical displacement is ahead of the mean temperatures in the upper surface and the lower surface of the main girder. Moreover, the time-lag effect between vertical displacement and the mean temperature in the upper surface of the main girder is more remarkable. As displayed in Fig. 8, longitudinal displacement lags behind the mean temperatures in the main arch rib and suspender and is ahead of the mean temperature in the upper surface of main girder. The time-lag effect between longitudinal displacement and the mean temperature in the lower surface of main girder in Fig. 7 is inconspicuous. In short, the time-lag effect dependents on

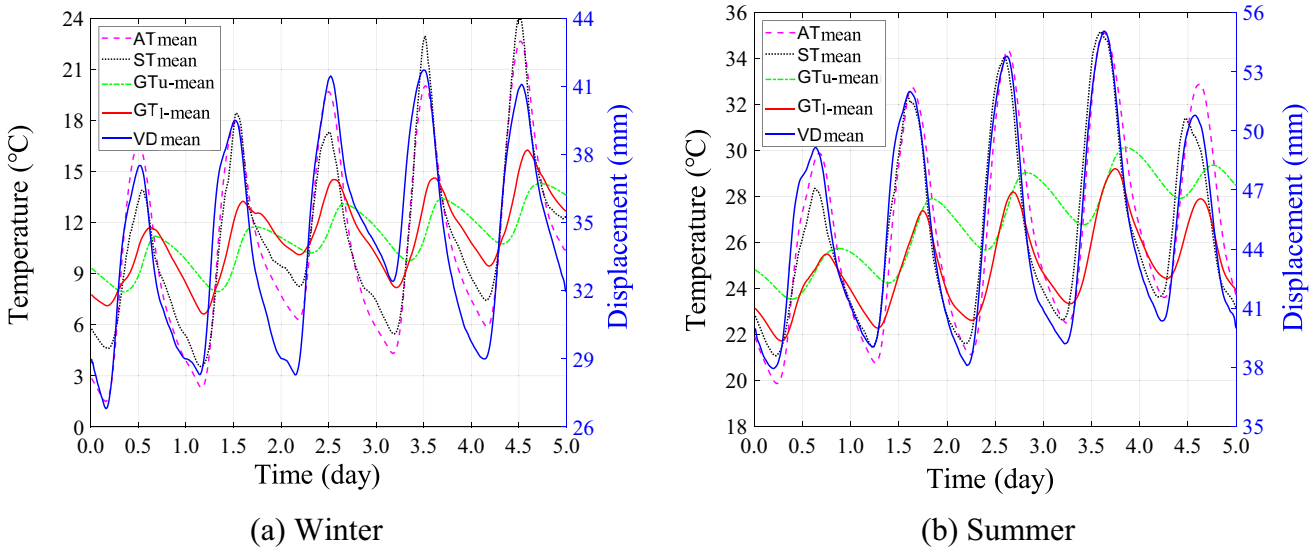

Fig. 7 Time histories of mean temperature and vertical displacement

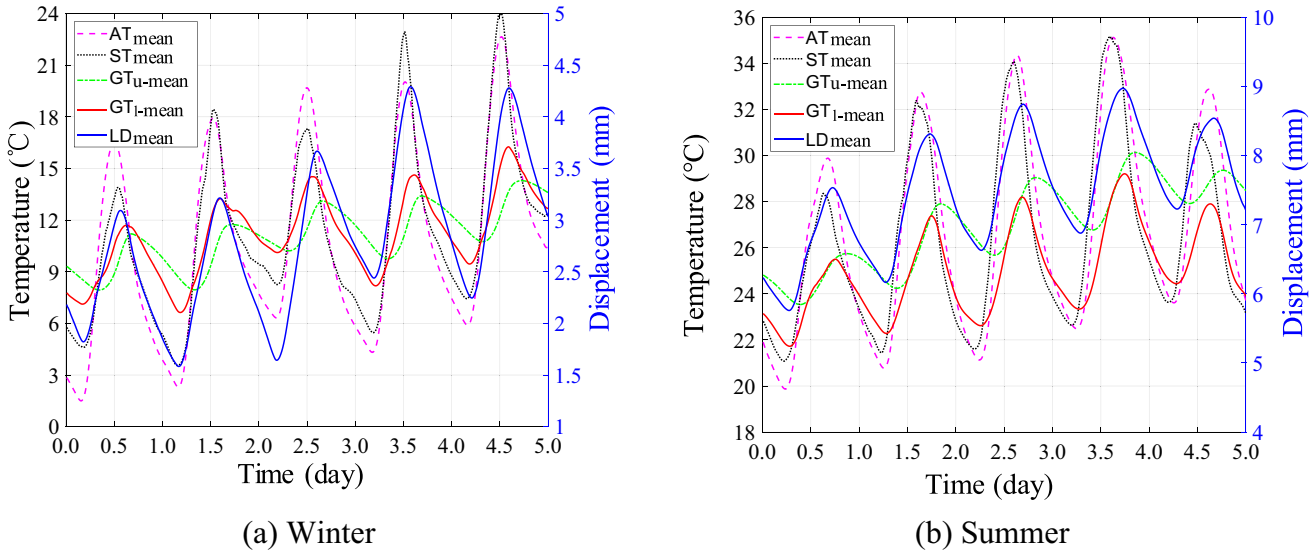

Fig. 8 Time histories of mean temperature and longitudinal displacement

the picked temperature and displacement variables and the selected time instance.

Focusing on the mean temperatures themselves in different bridge components, it can be observed that the change of different mean temperatures is asynchronous and the phase difference among mean temperatures is notable. Taking the heat exchange features of materials and geometric configurations of components into account, the main arch rib and suspender have similar heat exchange speed with ambient air because both of the them are made of steel and have small cross sections. As a consequence, the change of temperatures in the main arch rib and suspender is almost synchronous. On the contrary, the large amount of air in the box of the main girder results in lower heat exchange speed of the main girder than that of the main arch rib and suspender. As a result, the change of temperatures in the upper and lower surface lags behind that of the main arch rib and suspender. Furthermore, the upper surface of the main girder is in close contact with the concrete bridge deck with low thermal conductivity, which results in that the change of temperature in the upper surface of the main girder is the slowest.

The Kendall correlation coefficient, which measure the correlation of two sequences even if they do not obey the Gaussian distribution, among various mean temperatures and thermal displacements are calculated and listed in Table 2. Vertical displacement has high Kendall correlation coefficients with the mean temperatures in the main arch rib and suspender and low Kendall correlation coefficients with the mean temperatures in the upper and lower surface of the main girder, which indicates that the vertical displacement is governed by the mean temperatures in the main arch rib and suspender. Therefore, there should be no time-lag effect between vertical displacement and the

Table 2 Kendall correlation coefficients between mean temperatures and thermal displacements

Variables	Vertical displacement		Longitudinal displacement	
	Winter	Summer	Winter	Summer
AT_{mean}	0.94	0.93	0.13	0.19
ST_{mean}	0.92	0.89	0.16	0.18
GT_{u-mean}	0.15	0.19	0.47	0.42
GT_{l-mean}	0.43	0.46	0.94	0.95

mean temperatures in the main arch rib and suspender, as shown in Fig. 7. The asynchrony of the mean temperatures in the main arch rib and suspender and the mean temperatures in the upper and lower surface of the main girder results in the time-lag effect between vertical displacement and the mean temperatures in the upper and lower surface of the main girder. Similarly, the high Kendall correlation coefficient between longitudinal displacement and the mean temperature in the lower surface of the main girder illustrates that longitudinal displacement is dominated by the mean temperature in the lower surface of the main girder. As a result, there is no time-lag effect between them. And the mean temperature in the lower surface of the main girder lags behind the mean temperatures in the main arch rib and suspender and is ahead of the mean temperature in the upper surface of the main girder, as shown in Fig. 8, which leads to the remarkable time-lag effect of the longitudinal displacement. Finally, the unsynchronization of the mean temperatures in the main arch rib and suspender and the mean temperature in the lower surface of the main girder leads to the unsynchronization

of vertical displacement and longitudinal displacement, respectively, controlled by them.

3 Compensation method for the time-lag effect

In many SHM systems, only several temperature sensors are employed [23, 28]. There is not enough information to distinguish which is the dominant temperature for a certain displacement. Moreover, the dominant temperature for a certain displacement may be difficult to extract because of the complicated load and heat transfer. The environmental, effective or mean temperature is arbitrarily used to model the temperature-displacement correlation. In this instance, the time-lag effect is unavoidable and the model error may be unacceptable. Therefore, effective compensation method becomes necessary to eliminate the time-lag effect and enhance the correlation. The general compensation method without special processing for monitored data is proposed in this paper.

Mathematically, long-term monitored temperature and displacement results are typical functional data, so they can be processed by functional data analysis methods. It is supposed that the time histories of temperature and thermal displacement are represented by two functions $f_1(t)$ and $f_2(t)$, respectively, where t denotes time. The compensation of the time-lag effect is equivalent to the alignment or registration of the two functions $f_1(t)$ and $f_2(t)$. The core of function alignment is to separate amplitude variation from phase variation by the warping function, i.e., match peaks and valleys of the function [29].

Being different from general function alignment, in which functions are smooth, the smoothness of monitored temperature and thermal displacement is hard to ensure because of sudden climate changes and measurement errors. The Bayesian method, which has the capability to comprehensively explore the parameter space of the warping function and avoid the discretization of the infinite dimensional parameter space until the last step by incorporating prior knowledge [30], is thus integrated into the alignment to improve robustness and accuracy. In addition, a novel Z-mixture preconditioned Crank-Nicolson (pCN) algorithm is employed to effectively rank the posterior distribution on the space of the warping function.

3.1 Function space transformation

The long-term monitored temperature and thermal displacement are separated by day to meet the corresponding arrangement of the functional data analysis. The daily

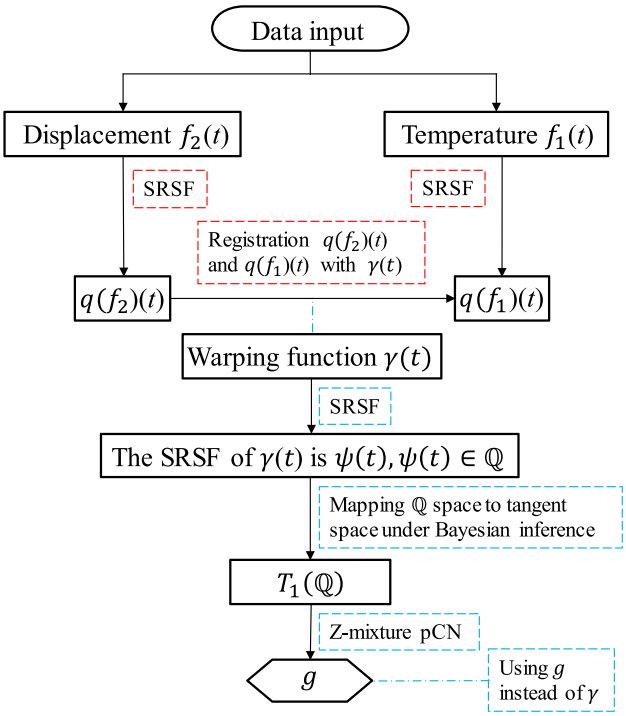

Fig. 9 Procedure of the time-lag effect compensation

temperature-displacement pair is aligned independently. Then, without loss of generality, the time interval [0 h, 24 h] is mapped linearly to [0, 1]. The collection that $f_1(t)$ and $f_2(t)$ belong to is represented by $\mathcal{F}$. The collection $\mathcal{F}$ has the property of $\mathcal{F} = \{f(t) : [0,1] \to \mathbb{R}\}$, where $\mathbb{R}$ is the real number set. The aim of the alignment of $f_1(t)$ and $f_2(t)$ is to find an optimal warping function $\gamma(t)$ to minimize the time-lag of $f_1(t)$ and $f_2(t) \circ \gamma(t)$ or $f_1(t) \circ \gamma(t)$ and $f_2(t)$, where $\circ$ represents the composite operation; $\gamma(t) \in \Gamma$, Γ is the set of boundary-preserving diffeomorphisms with the unit interval [0, 1]. Γ belongs to the Lie group with the identity element $\gamma_{id}(t) = t$ and is defined as [30]

$$\Gamma = \{\gamma : [0,1] \to [0,1] | \gamma(0) = 0, \gamma(1) = 1\} \tag{8}$$

Unfortunately, this alignment is neither symmetric nor positive definite, which is

$$inf_{\gamma(t)\in\Gamma} \|f_1(t), f_2(t) \circ \gamma_2(t)\| \neq inf_{\gamma(t)\in\Gamma} \|f_1(t) \circ \gamma_1(t), f_2(t)\| \tag{9}$$

where $\|\cdot\|$ represents the L_2 norm.

To cope with this problem, the square-root slope function (SRSF) is introduced [31]. The function $f(t)$ can be converted to

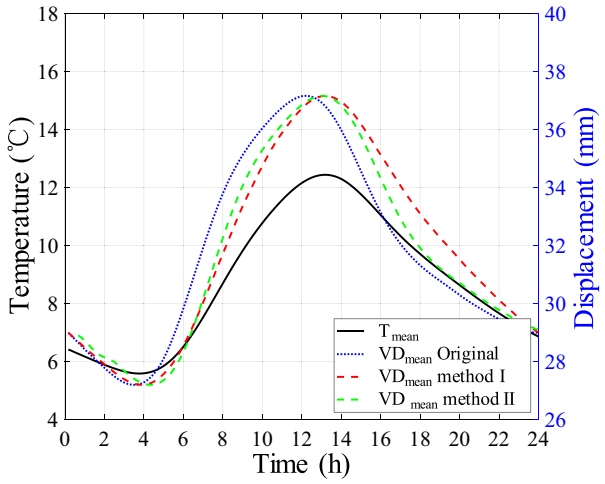

(a) Mean temperature vs. vertical displacement in winter

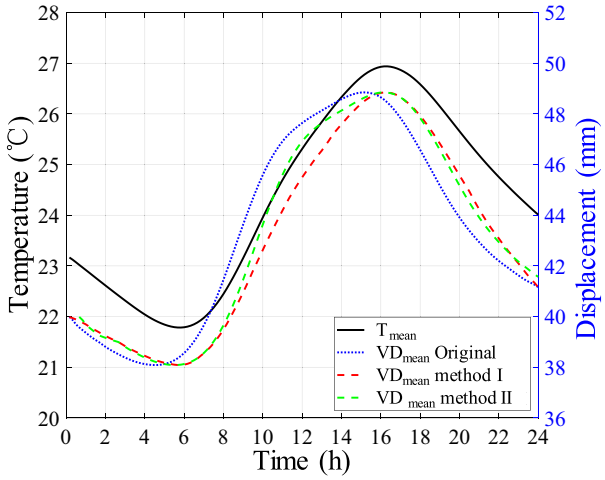

(b) Mean temperature vs. vertical displacement in summer

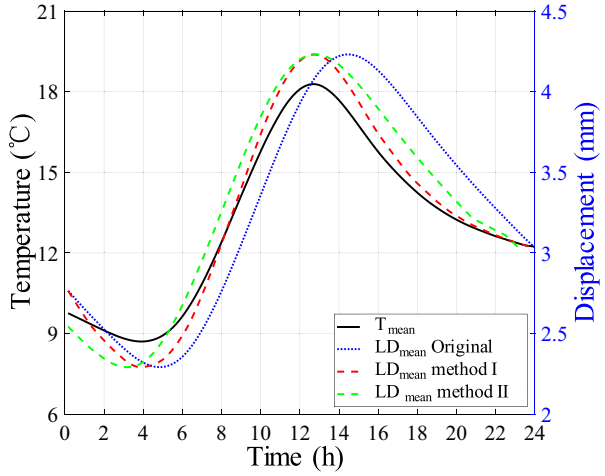

(c) Mean temperature vs. longitudinal displacement in winter

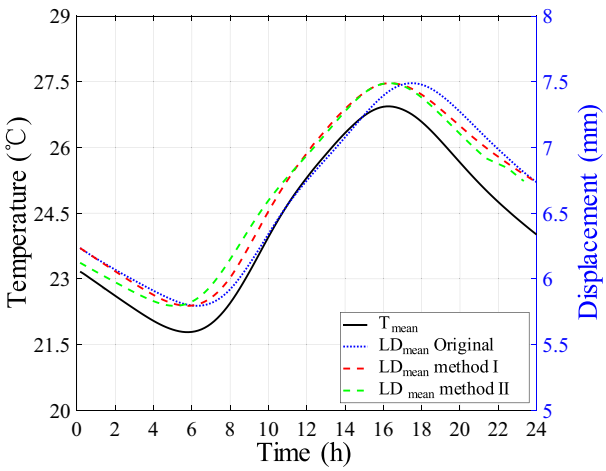

(d) Mean temperature vs. longitudinal displacement in summer

Fig. 10 Typical time histories of mean temperature and thermal displacement before and after compensation

$$q(f) : [0,1] \to \mathbb{R}, q(t) = sign(\dot{f}(t))\sqrt{|\dot{f}(t)|} \tag{10}$$

where $q(t)$ represents the SRSF of $f(t)$, $\dot{f}(t)$ is the derivative of $f(t)$, and $sign(\cdot)$ denotes the symbolic function.

According to the properties of Eq. (10) and its inverse transformation [32], the SRSF of $f(t) \circ \gamma(t)$ is equal to

$$(q,\gamma)(t) = q(\gamma(t))\sqrt{\dot{\gamma}(t)} \tag{11}$$

As a result, the following symmetric equation can be obtained.

$$\|q_1(t) - q_2(t)\| = \|(q_1,\gamma)(t) - (q_2,\gamma)(t)\| \tag{12}$$

where $q_1(t)$ and $q_2(t)$ are SRSFs of $f_1(t)$ and $f_2(t)$, respectively.

It can be seen from Eq. (12) that the warping function $\gamma(t)$ can solve the problem of symmetric alignment between $q_1(t)$ and $q_2(t)$. That is to say, if $q_1(t)$ is aligned with $q_2(t)$ by $\gamma(t)$, $q_2(t)$ is also aligned with $q_1(t)$ by the same $\gamma(t)$. Furthermore, $f_1(t)$ and $f_2(t)$ are aligned by the same warping function $\gamma(t)$ and the time-lag effect between $f_1(t)$ and $f_2(t)$ is eliminated. The collection of $q(t)$ is termed as a quotient space, represented by L_2/Γ.

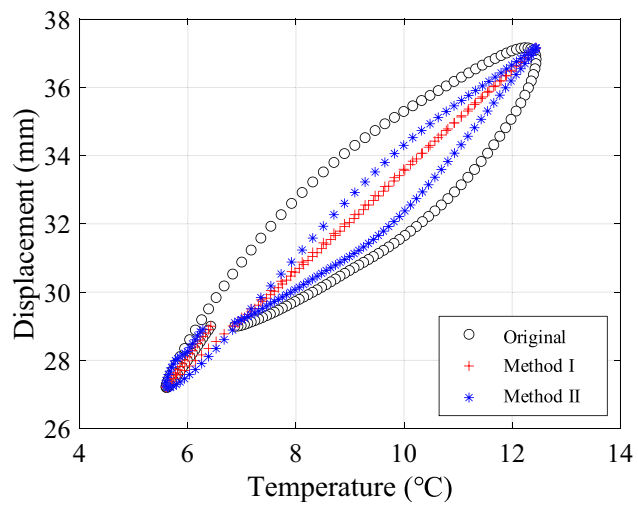

(a) Vertical displacement vs. mean temperature in winter

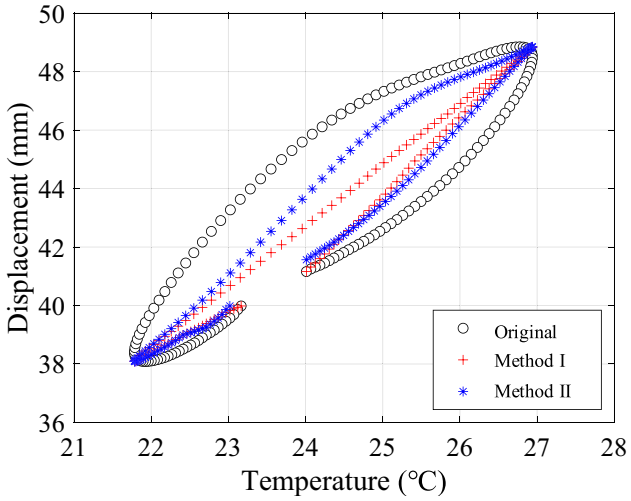

(b) Vertical displacement vs. mean temperature in summer

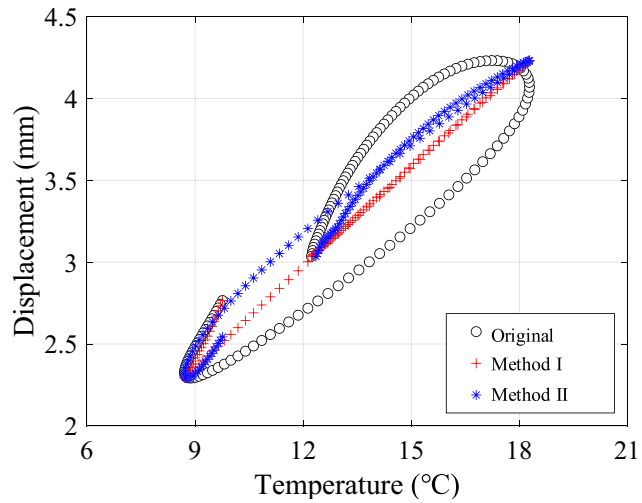

(c) Longitudinal displacement vs. mean temperature in winter

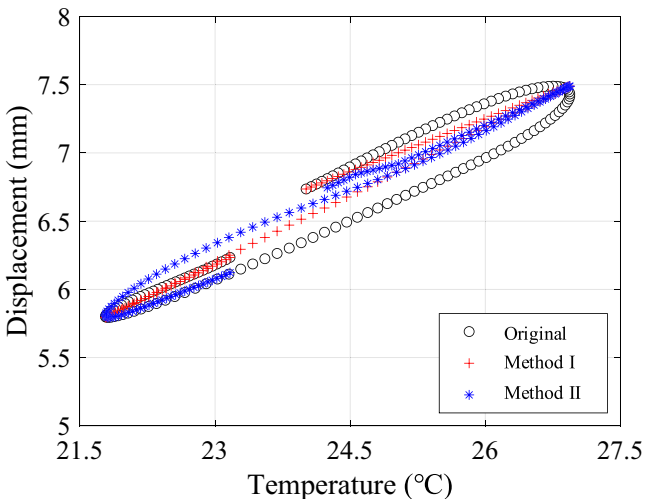

(d) Longitudinal displacement vs. mean temperature in summer

Fig. 11 Correlations between mean temperature and thermal displacement before and after compensation

However, the Bayesian function registration is difficult to operate in the quotient space for the reason that Γ is a nonlinear manifold. In order to incorporate the Bayesian function registration model to improve the alignment accuracy, the warping function $\gamma(t)$ should be mapped to the tangent space $T_1(\mathbb{Q})$, which is a linear space with the property of isometry and invertibility. The detailed derivation is listed in Appendix A [30, 31, 33, 34].

3.2 Bayesian model specification

As mentioned above, the alignment of $f_1(t)$ and $f_2(t)$ can be performed on the quotient space. The difference $q(f_1)(t) - q(f_2)(t)$ can be assumed as a standard multivariate Gaussian distribution. Using g instead of γ, the likelihood is reparametrized as follows:

$$q(f_2 \circ \gamma)(t) = q(f_2)\left\{\int_0^t exp_1^2(g)(s)ds\right\} exp_1(g)(t) \tag{13}$$

Table 3 Kendall correlation coefficients before and after compensation

Thermal displacement		Winter	Summer
Vertical displacement	Original	0.53	0.38
	Compensated by method I	0.95	0.92
	Compensated by method II	0.83	0.78
Longitudinal displacement	Original	0.51	0.42
	Compensated by method I	0.98	0.95
	Compensated by method II	0.80	0.82

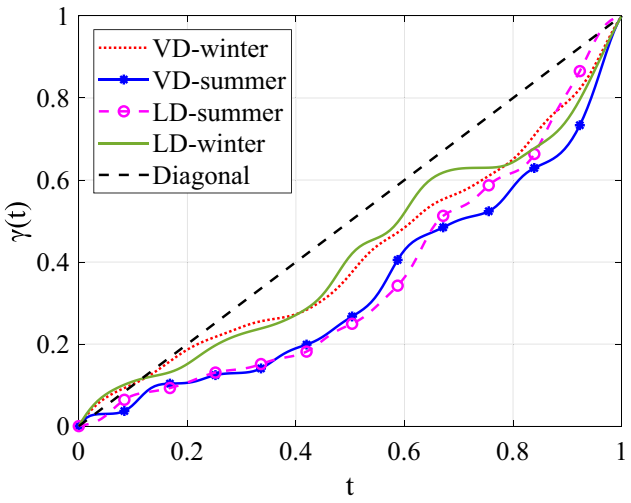

Fig. 12 Warping functions in case one

The prior distribution on g is restricted to a subset $\mathcal{H}$, which is defined by

$$g \in \mathcal{H} \subset \mathrm{T}_1(\mathbb{Q}) \iff exp_1(g) > 0 \tag{14}$$

The Bayesian model of the warping function is fully specified as.

$$\begin{aligned} &q(f_1)([t]) - q(f_2)\left\{\int_0^{[t]} exp_1^2(g)(s)ds\right\} exp_1(g)(t)|g, \\ &\sigma_1^2 \sim N(0_N, \sigma_1^2 I_N), \\ &g \sim \text{Gaussian}\left(0, \mathcal{C}_g; I_A\right), \\ &\sigma_1^2 \sim IG(a, b) \end{aligned} \tag{15}$$

where Gaussian $(\bullet, \bullet; I_A)$ represents the Gaussian process restricted to the domain $\mathcal{H}$, $\mathcal{C}_g$ is a prespecified covariance operator, $IG(\bullet, \bullet)$ denotes the inverse gamma distribution with determined constants a and b, $\sigma_1^2 I$ is the covariance matrix of the normal distribution, I denotes the identity matrix, and the subscript N is the length of the vector representing $f_1(t)$ and $f_2(t)$. The detailed derivation of this model can be referred to Lu et al. [30].

The solve of the prior and posterior distributions by the Z-mixture pCN algorithm is provided in Appendix B. The procedure for the time-lag effect compensation is shown in Fig. 9.

4 Method verification

Three cases are adopted to validate the proposed time-lag effect compensation method. Data in case one are those monitored results in Sect. 2. Data in case two and case three are obtained from two long-span cable-stayed bridges with steel truss main girders. In each case, the compensated method proposed in this paper and the compensated method by shifting a fixed time interval, which are termed as "method I" and "method II" in the following description, respectively, are applied and compared.

4.1 Case one

By using the data in Sect. 2, typical time histories of the mean temperature and thermal displacement before and after compensation in 24 h is shown in Fig. 10. The fixed time intervals in method II are selected as -50 min, -60 min, 80 min, 70 min so that peaks of these curves are accurately aligned. As can be seen, the time-lag effect is no longer observed after compensated by the method proposed in this paper (method I), while the time-lag effect still exists after compensated by the method of shifting a fixed time interval (method II). Because the time-lag effect change with time, there is not a fixed time to meet the requirement that the peak and valley of mean temperature and thermal displacement are aligned simultaneously. Further, the correlation between mean temperature and thermal displacement before and after compensation are plotted in Fig. 11. It can be easily found that the thermal displacement compensated by method I has a stronger correlation with the mean temperature. The feature of the hysteresis loop can still be detected, even if the thermal displacement is compensated by method II. The superiority of the compensation method proposed in this paper has been demonstrated.

The Kendall correlation coefficients between mean temperature and thermal displacement before and after compensation are calculated and listed in Table 3. After the time-lag effect is compensated by method I, the essential relationship between mean temperature and thermal displacement is revealed and the linearity between them is significantly enhanced. The Kendall correlation coefficients are

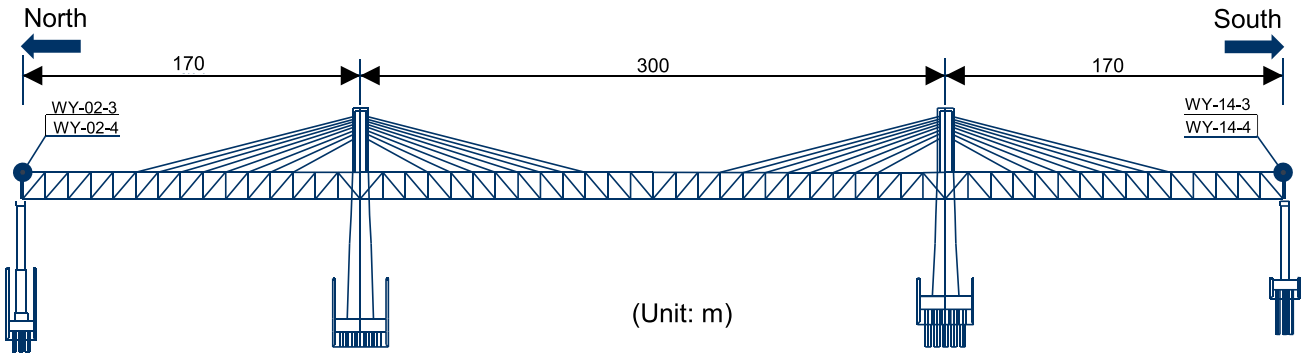

(a) Elevation view of the bridge

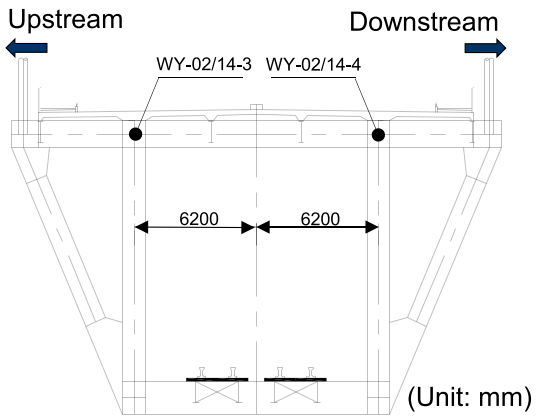

(b) Distribution of displacement sensors

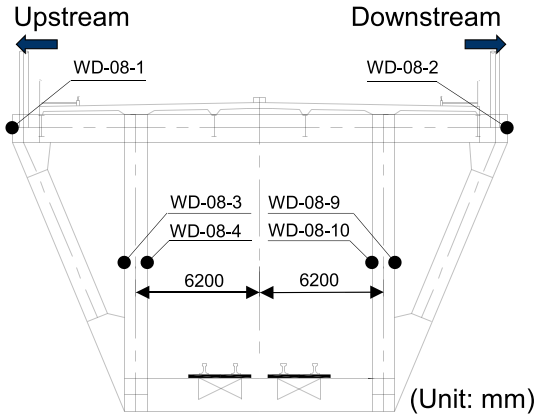

(c) Distribution of temperature sensors

Fig. 13 Layout of displacement and temperature sensors on the bridge

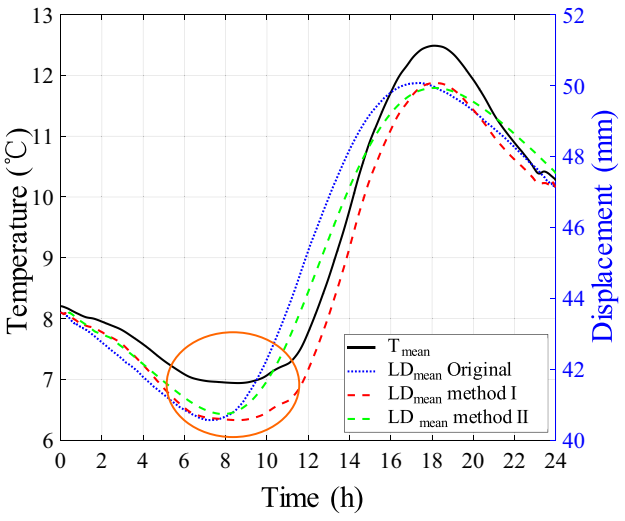

(a) Time histories

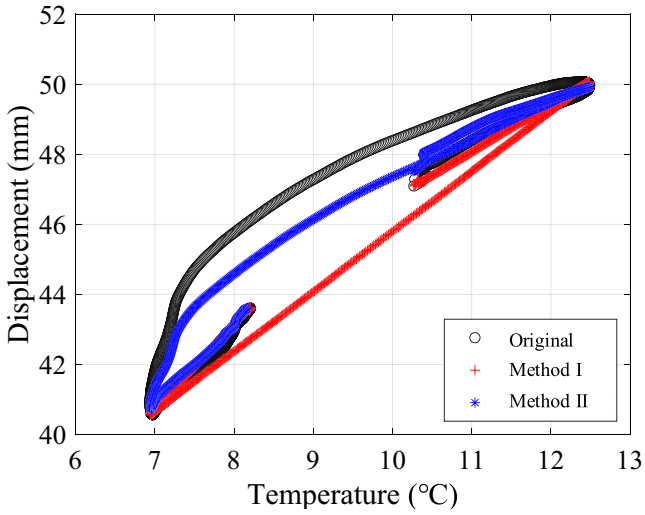

(b) Correlations

Fig. 14 Comparison of mean temperature and longitudinal displacement before and after compensation in case two

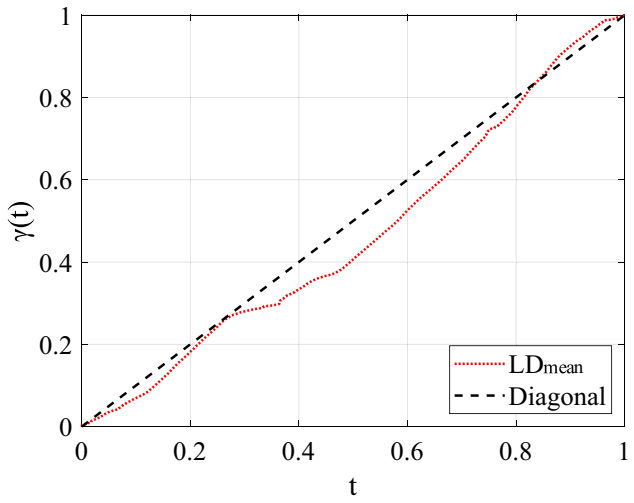

Fig. 15 Warping function in case two

greatly improved (i.e. from 0.38 to 0.92). On the contrary, the improvement of the linearity between mean temperature and thermal displacement compensated by method II is limited (i.e. from 0.38 to 0.78) for the reason that the time-lag effect has not been completely eliminated. The effectiveness of the proposed compensation method is verified again. These compensated mean temperature and thermal displacement would result in more accurate temperature–displacement models and more reliable displacement-based safety evaluation.

The warping functions, which are adopted to align these functional data in Fig. 10, are plotted in Fig. 12. In the figure, the time interval [0 h, 24 h] is mapped linearly to [0, 1] and the distance between the warping function and the diagonal can measure the time-lag effect. The larger the distance is, the more obvious the time-lag effect is. It can be found that, the time-lag effects are different on different days and at different time instances. Flexible time compensation can better remove the time-lag effect.

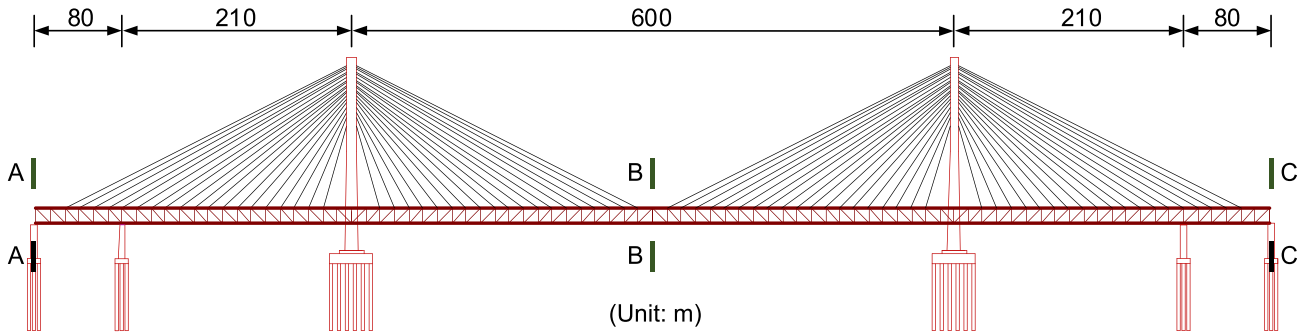

(a) Elevation view of the bridge

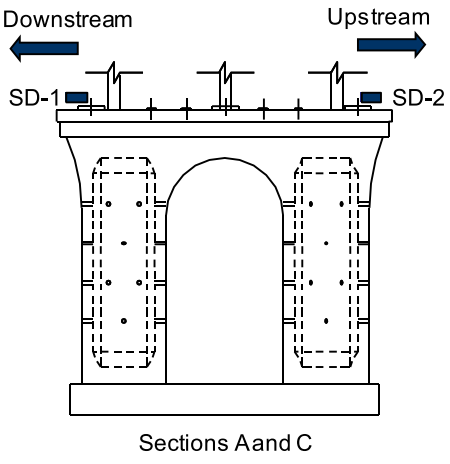

(b) Distribution of displacement sensors

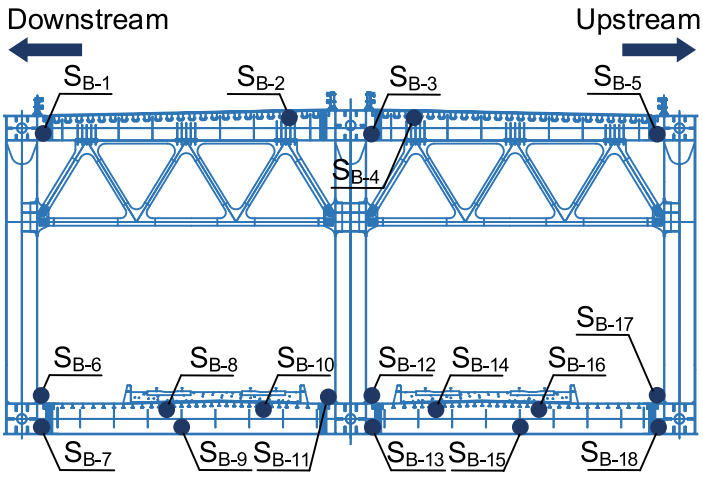

(c) Distribution of temperature sensors

Fig. 16 Layout of displacement and temperature sensors on the bridge

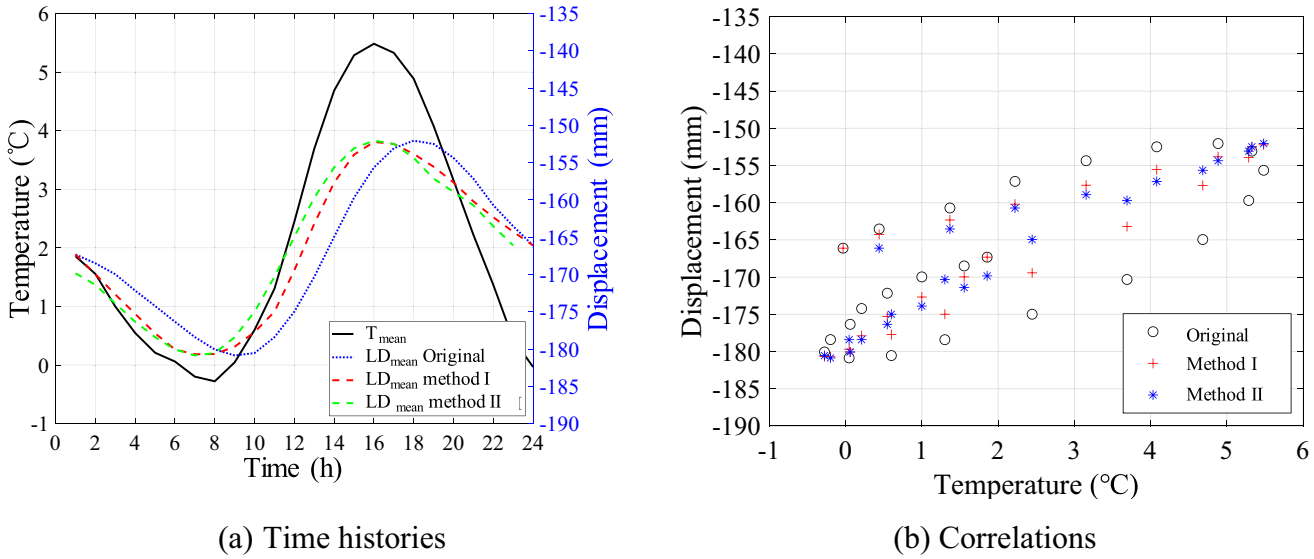

(a) Time histories (b) Correlations

Fig. 17 Comparison of mean temperature and longitudinal displacement before and after compensation in case three

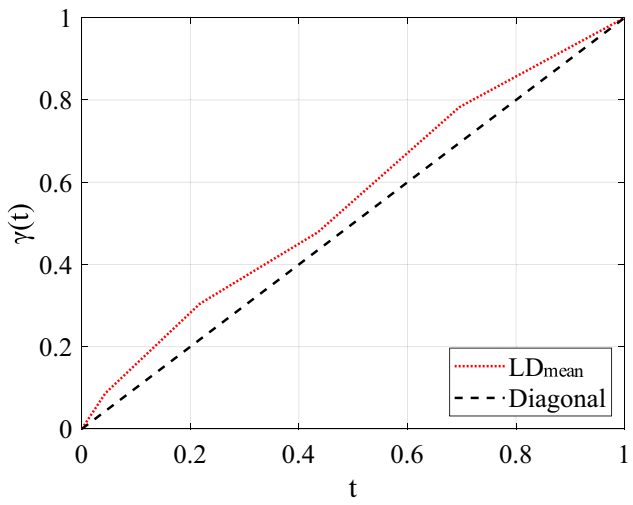

Fig. 18 Warping function in case three

4.2 Case two

The data used for verification in this case were recorded by a SHM system equipped on a long-span cable-stayed bridge. The main span and two equal side spans are 300 m and 170 m, respectively. The elevation view of the bridge and the arrangement of longitudinal displacement sensors are shown in Fig. 13(a). The longitudinal displacement is monitored by sensors located on two ends of the main girder and the structural temperature is monitored by sensors located on the cross-section, as plotted in Fig. 13b, c**.**

The mean values of all longitudinal displacement sensors and the mean values of all temperature sensors in 24 h, which are referred as T_{mean} and LD_{mean}, respectively, are calculated and adopted to analyze. The longitudinal displacement and temperature are averaged in 1 min. The time histories and correlations before and after compensation are displayed in Fig. 14. The Kendall correlation coefficient increases from 0.44 to 0.95 (method I) and 0.79 (method II). And the warping function is shown in Fig. 15. It can be found that the time-lag effect can be completely eliminated by method I. There is still a time-lag between temperature and longitudinal displacement compensated by method II in the valley of the curve, as marked by a circle in Fig. 14. The mean temperature has a stronger correlation with the thermal displacement compensated by method I than that compensated by method II. The superiority of the proposed compensation method has been proven again. Similarly, the lag time also changes with time, measuring from the distance between the warping function and the diagonal in Fig. 15.

4.3 Case three

The data monitored from the bridge of case three are also employed. As shown in Fig. 16, the longitudinal displacement of the main girder is monitored by four displacement sensors located on 2 main girder ends and the structural

temperature of the cross-section in the middle span is carefully measured by 18 temperature sensors.

Being similar to case two, the mean values of all longitudinal displacement sensors and the mean values of all temperature sensors in 24 h, which are also referred as T_{mean} and LD_{mean}, respectively, are employed. The longitudinal displacement and temperature are averaged in one hour. The results are shown in Figs. 17 and 18. It can be seen from these figures that no matter whether the mean temperature and thermal displacement are positive or negative, the time-lag effect can be compensated by method I. The Kendall correlation coefficient is improved from 0.38 to 0.93 (method I) and 0.75 (method II). The linearity between the mean temperature and thermal displacement compensated by method I is better than that performed by method II.

5 Conclusions

The time-lag effect is a key factor reducing the temperature–displacement correlation. In this paper, based on long-term monitoring data of temperature and displacement from three different bridges, the typical characteristics of the time-lag effect are investigated and a compensation method is proposed. The main conclusions are drawn as follows:

(1) The proposed compensation method originated from the Bayesian function registration model and the Z-mixture preconditioned Crank-Nicolson algorithm has the capability to completely eliminate the time-lag effect without any prior knowledge. Furthermore, the proposed compensation method is applicable to positive or negative data measured from various types of long-span bridges and pre-correlation analysis of data is unnecessary.

(2) Compared to the traditional method, which eliminates the time-lag effect by shifting a fixed time interval, the compensation method proposed in this paper can cope with the time-dependent time-lag effect and exhibits superior adaptability. The Kendall correlation coefficients between temperature and thermal displacement compensated by the proposed method is higher and the correlation is stronger.

Appendix A

The SRSF of the warping function $\gamma(t)$ is

$$\psi(t) = \sqrt{\dot{\gamma}(t)} \tag{A.1}$$

Since $\gamma(0) = 0$, this mapping operation is invertible. One typical feature of $\psi(t)$ is that it has unit L_2 norm as follows

$$\|\psi(t)\|^2 = \int_0^1 \psi(t)^2 dt = \int_0^1 \dot{\gamma}(t)^2 dt = \gamma(1) - \gamma(0) = 1 \tag{A.2}$$

The resulting space $\mathbb{Q}$ ($\psi(t) \in \mathbb{Q}$) is the positive orthant of the unit sphere in the Hilbert space L_2. On the space, the distance can be defined by the arc-length, and the mapping operation also has the property of isometry. Although the SRSF transformation simplifies the complicated geometry of Γ, the space $\mathbb{Q}$ is yet to be linear and cannot meet the requirement of the Bayesian function registration. As a result, the further transformation is required.

The space $\mathbb{Q}$ is mapped onto a tangent space. The identity element $\gamma_{id}(t) \in \Gamma$ accordingly maps to a constant function $1 \in \mathbb{Q}$. The tangent space at this specified point is

$$T_1(\mathbb{Q}) = \left\{ g : [0,1] \to \mathbb{R} | \langle g, 1 \rangle = \int_0^1 g(t) dt = 0 \right\} \tag{A.3}$$

where g is the representation of the warping function $\gamma(t)$ in the tangent space. One way to connect $\mathbb{Q}$ and $T_1(\mathbb{Q})$ is via the exponential map and inverse exponential map, which are defined as

$$T_1(\mathbb{Q}) \to \mathbb{Q} exp_1(g) = cos(\|g\|) + \frac{sin(\|g\|)}{\|g\|} g, g \in T_1(\mathbb{Q}) \tag{A.4}$$

$$\mathbb{Q} \to T_1(\mathbb{Q}) exp_1^{-1}(\psi) = \frac{\theta}{sin(\theta)}[\psi - cos(\theta)], \quad \theta = arccos(\langle 1, \psi \rangle), \psi \in \mathbb{Q} \tag{A.5}$$

where θ is the vectorial angle between 1 and ψ.

Appendix B

In Eq. (15), the prior and posterior distributions of $\left(g, \sigma_1^2\right)$ are probability measures defined on the product space $T_1(\mathbb{Q}) \times \mathbb{Q}$. Specifically, the prior measure is the product measure $\mu_0 \equiv \text{Gaussian}\left(0, \mathcal{C}_g; I_A\right) \times IG(a, b)$ and the posterior measure μ is absolutely continuous with respect to the prior measure. By using Bayesian formula, the Radon-Nikodym derivative of the posterior measure μ is

$$\frac{d\mu}{d\mu_0}\left(g, \sigma_1^2\right) \propto L\left(g, \sigma_1^2 \mid f_1, f_2\right) \tag{B.1}$$

where $L\left(\bullet, \bullet \mid f_1, f_2\right)$ is the likelihood function given by

$$L\left(g, \sigma_1^2 \mid f_1, f_2\right) \propto \left(\frac{1}{\sigma_1^2}\right)^{N/2} exp\left\{ -\frac{1}{2\sigma_1^2} SSE(g) \right\} \tag{B.2}$$

$$SSE(g) = \sum_{i=1}^{N} \left(q(f_1)(t_i) - q(f_2) \left(\int_0^{t_i} exp_1^2(g)(s)\mathrm{d}s \right) \times exp_1(g)(t_i) \right)^2 \tag{B.3}$$

The Metropolis in Gibbs algorithm could be adopted to search the posterior distribution given by Eq. (B.1). At each iteration, the component σ_1^2 is updated with values extracted from the conditional distribution as follows:

$$\sigma_1^2 \mid g, f_1, f_2 \sim IG\left(\frac{N}{2} + a, \frac{1}{2} SSE(g) + b \right) \tag{B.4}$$

While the functional component g is updated by the Metropolis–Hastings step. In this step, the functional component g could be obtained by the Z-mixture pCN algorithm, which is

$$g' \sim \sum_{z=1}^{Z} p_z Gaussian\left(g\sqrt{1-\beta_z^2}, \beta_z^2 \mathcal{C}_g; \mathrm{I_A} \right) \tag{B.5}$$

where g' is the updated functional component g.

Acknowledgements This research work was supported by the National Natural Science Foundation of China (Grant Nos. 51978243). The authors would like to express their appreciation to Prof. Chunfeng Wan and Dr. Huachen Jiang from Southeast University for their valuable suggestions.

Data availability The data that support the findings of this study are available on request from the corresponding author. The data are not publicly available due to privacy or ethical restrictions.

Declarations

Conflict of interest The author(s) declared no potential conflicts of interest with respect to the research, authorship, and/or publication of this article.

References

1. Svendsen BT, Frøseth GT, Øiseth O, Rønnquist A (2021) A data-based structural health monitoring approach for damage detection in steel bridges using experimental data. J Civ Struct Heal Monit 12:101–115. https://doi.org/10.1007/s13349-021-00530-8
2. Mishra M, Barman SK, Maity D, Maiti DK (2019) Ant lion optimisation algorithm for structural damage detection using vibration data. J Civ Struct Heal Monit 9:117–136. https://doi.org/10.1007/s13349-018-0318-z
3. Ye S, Lai X, Bartoli I, Aktan AE (2020) Technology for condition and performance evaluation of highway bridges. J Civ Struct Heal Monit 10:573–594. https://doi.org/10.1007/s13349-020-00403-6
4. Shan J, Wang L, Loong CN, Zhou Z (2023) Rapid seismic performance evaluation of existing frame structures using equivalent SDOF modeling and prior dynamic testing. J Civ Struct Heal Monit 13:749–766. https://doi.org/10.1007/s13349-023-00677-6
5. Yarnold MT, Moon FL, Aktan AE (2015) Temperature-based structural identification of long-span bridges. J Struct Eng 141(11):04015027. https://doi.org/10.1061/(ASCE)ST.1943-541X.0001270
6. Liu Y, Deng Y, Cai C (2015) Deflection monitoring and assessment for a suspension bridge using a connected pipe system: a case study in China. Struct Control Health Monit 22:1408–1425. https://doi.org/10.1002/stc.1751
7. Han Q, Ma Q, Xu J, Liu M (2021) Structural health monitoring research under varying temperature condition: a review. J Civ Struct Health Monit 11(1):149–173. https://doi.org/10.1007/s13349-020-00444-x
8. Xu Y, Chen B, Ng CL, Wong K, Chan W (2010) Monitoring temperature effect on a long suspension bridge. Struct Control Health Monit 17:632–653. https://doi.org/10.1002/stc.340
9. Zhou Y, Xia Y, Fujino Y, Yamaguchi K (2021) Analytical formulas of thermal deformation of suspension bridges. Eng Struct 238:112228. https://doi.org/10.1016/j.engstruct.2021.112228
10. Li LF, Chen B, Zhou LR, Xia Q, Zhou Y, Zhou XQ, Xia Y (2023) Thermal behaviors of bridges—a literature review. Adv Civil Eng 26(6):985–1010. https://doi.org/10.1177/13694332231153976
11. Potgieter IC, Gamble WL (1989) Nonlinear temperature distributions in bridges at different locations in the United States. PCI J 34(4):80–103
12. Ni YQ, Hua XG, Fan KQ, Ko JM (2005) Correlating modal properties with temperature using long-term monitoring data and support vector machine technique. Eng Struct 27:1762–1773. https://doi.org/10.1016/j.engstruct.2005.02.020
13. Ni YQ, Hua XG, Wong K, Ko JM (2007) Assessment of bridge expansion joints using long-term displacement and temperature measurement. J Perform Constr Facil 21:143–151. https://doi.org/10.1061/(ASCE)0887-3828(2007)21:2(143)
14. Catbasa FN, Susoyb M, Frangopol DM (2008) Structural health monitoring and reliability estimation: long span truss bridge application with environmental monitoring data. Eng Struct 30:2347–2359. https://doi.org/10.1016/j.engstruct.2008.01.013
15. Kromanis R, Kripakaran P (2014) Predicting thermal response of bridges using regression models derived from measurement histories. Comput Struct 136:64–77. https://doi.org/10.1016/j.compstruc.2014.01.026
16. Yang D, Yi T, Li H, Zhang Y (2018) Monitoring and analysis of thermal effect on tower displacement in cable-stayed bridge. Measurement 115:249–257. https://doi.org/10.1016/j.measurement.2017.10.036
17. Zhou, G, Yi T, Chen B, Chen X (2018) Modeling Deformation induced by thermal loading using long-term bridge monitoring data. J Perform Constr Facil 32(3): 04018011. https://doi.org/10.1061/(ASCE)CF.1943-5509.0001154.
18. Battista N, Brownjohn J, Tan H, Koo KY (2015) Measuring and modelling the thermal performance of the Tamar Suspension Bridge using a wireless sensor network. Struct Infrastruct Eng 11(2):176–193. https://doi.org/10.1080/15732479.2013.862727
19. Hu J, Wang L, Song X (2020) Field monitoring and response characteristics of longitudinal movements of expansion joints in long-span suspension bridges. Measurement 162:107933. https://doi.org/10.1016/j.measurement.2020.107933
20. Westgate R, Koo KY, Brownjohn J (2015) Effect of solar radiation on suspension bridge performance. J Bridge Eng 20(5):04014077. https://doi.org/10.1061/(ASCE)BE.1943-5592.0000668
21. Wang ZW, Zhang WM, Zhang YF, Liu Z (2022) Temperature prediction of flat steel box girders of long-span bridges utilizing in situ environmental parameters and machine learning. J Bridge Eng 27:04022004. https://doi.org/10.1061/(ASCE)BE.1943-5592.0001840
22. Ju H, Zhai W, Deng Y, Chen M, Li A (2023) Temperature time-lag effect elimination method of structural deformation monitoring

data for cable-stayed bridges. Case Stud Thermal Eng 42:102696. https://doi.org/10.1016/j.csite.2023.102696
23. Guo T, Liu J, Zhang Y, Pan S (2015) Displacement monitoring and analysis of expansion joints of long-span steel bridges with viscous dampers. J Bridge Eng 20(9):04014099. https://doi.org/10.1061/(ASCE)BE.1943-5592.0000701
24. Yang D, Yi T, Li H, Zhang Y (2018) Correlation-based estimation method for cable-stayed bridge girder deflection variability under thermal action. J Perform Constr Facil 32(5):04018070. https://doi.org/10.1061/(ASCE)CF.1943-5509.0001212
25. Zhou, G, Yi T, Chen B (2017) Innovative Design of a Health Monitoring System and Its Implementation in a Complicated Long-Span Arch Bridge. J Aeros. Eng B4016006. https://doi.org/10.1061/(ASCE)AS.1943-5525.0000603.
26. Roeder CW (2002) Thermal movement design procedure for steel and concrete bridges. University of Washington, Seattle, WA, USA
27. Aashto (2017) LRFD-8 AASHTO LRFD bridge design specifications. Washington DC, USA: AASHTO.
28. Li N, Zhang X, Zhou X, Leng J, Liang Z, Zheng C, Sun X (2008) Introduction of structural health and safety monitoring warning systems for Shenzhen-Hongkong western corridor Shenzhen bay bridge. Health Monitoring Struct Biol Syst 6935:69351L-L69361. https://doi.org/10.1117/12.775827
29. Tucker JD, Wu W, Srivastava A (2013) Generative models for functional data using phase and amplitude separation. J Comput Stat Data Anal 61:50–66. https://doi.org/10.1016/j.csda.2012.12.001
30. Lu Y, Herbei R, Kurtek S (2017) Bayesian registration of functions with a gaussian process Prior. J Comput Graph Statist 26(4):894–904. https://doi.org/10.1080/10618600.2017.1336444
31. Tucker JD, Wu W, Srivastava A (2014) Analysis of proteomics data: phase-amplitude separation using an extended Fisher -Rao metric. Electron J Statist 8(2):1724–1733. https://doi.org/10.1214/14-EJS900B
32. Srivastava, A, Wu W, Kurtek S, Klassen E, Marron J S (2011) Registration of functional data using fisher-rao metric. arXiv preprint, arXiv 1103.3817.
33. Srivastava, A, Jermyn I, Joshi S (2007) Riemannian analysis of probability density functions with applications in vision. IEEE CVPR. 1–8. https://doi.org/10.1109/CVPR.2007.383188.
34. Cotter SL, Roberts GO, Stuart AM, White D (2013) MCMC methods for functions: modifying old algorithms to make them faster. Statist Sci 28:424–446. https://doi.org/10.1214/13-STS421